Progress In Electromagnetics Research M, Vol. 33, 251–262, 2013

THE RESEARCH ON SHORT-RANGE TARGET HOLOGRAPHIC IMAGING ALGORITHM

Li Zhu*, Xing-Guo Li, and Ben-Qing Wang

Department of Detection and Control Engineering, Institute of Electro-Optical, Nanjing University of Science and Technology, Nanjing 210094, China

Abstract—Because the oversized, ultra short-range and arbitrary-shape goals cannot be imaged by Fourier transform algorithm, a Boundary Element Method (BEM) is presented for short-range millimeter wave holographic imaging. Through the discrete boundary integral equation, the discrete electromagnetic fields on the source surface and holographic surface are obtained. They are linked by a transfer matrix. Finally, the discrete electromagnetic fields obtain target holographic image. Due to the complexity of the transfer matrix, the Distributed Source Boundary Point Method (DSBPM) is introduced to calculate it, which greatly simplifies the calculation process. The simulation experiments of three-dimensional hemisphere imaging show the sensitivity of the imaging algorithm to test error, and regularization method has been proposed. The actual measurement of the four small metal balls verifies the validity of the imaging algorithm for large target imaging. The imaging results show that holographic imaging of the boundary element method can obtain high resolution and high amplitude accuracy.

1. INTRODUCTION

Holography technology arose in optical field and later was introduced into the microwave and acoustic fields. The characters of microwave and near-field acoustic holography were introduced into short-range millimeter wave holographic imaging. McMakin et al. and Sheen et al., who work in the Pacific Northwest National Laboratory, lead the research in the world. They have developed a millimeter holographic three-dimensional imaging system based on cylindrical scan [1–3]. The

Received 6 September 2013, Accepted 21 October 2013, Scheduled 8 November 2013
* Corresponding author: Li Zhu (hfjr317-zl@vip.sina.com).

basic algorithm of short-range millimeter wave holographic imaging is Fourier transform algorithm (FT), which was applied by the above-mentioned imaging system. But FT algorithm has many limits, such as the requirements of the source surface and the hologram surface conformal, the hologram surface 2 times larger than the source surface, etc. It is difficult to obtain a large size target imaging.

BEM is presented for short-range millimeter wave holographic imaging, which can overcome the shortcomings of FT and achieve analysis and reconstruction of arbitrary-shape targets [4, 5]. Due to the complexity of the transfer matrix, the singularity and non-unique solution of integration, etc., DSBPM is introduced to simplify the calculation and improve the imaging efficiency. The basic principles of BEM and DSBPM are introduced in this paper, and then their characters are discussed in detail. Finally, different targets imaging are simulated.

2. BEM IMAGING ALGORITHM

The Helmholtz equation is transformed into the boundary integral equation by the Green theorem, the transfer relation about the source surface, and the holographic surface is established. Known and unknown quantities are concentrated on the boundary, and the imaging dimension is reduced. Through discreting the integral equation, the transfer matrix can be obtained, and arbitrary targets can be reconstructed. It is the basic idea of BEM. Based on the scalar diffraction theory, holographic imaging of quasi-monochromatic field is discussed [6]. Assuming that electromagnetic wave λ propagates in a homogeneous medium, the complex amplitude E meets the Helmholtz equation:

$$\left(\nabla^2 + K^2\right) E = 0 \tag{1}$$

where ∇^2 is the Laplace operator, K the wave number, and $K = 2\pi/\lambda$. In the case of Sommerfeld radiation, the electromagnetic field $E(p)$ of any point p in space can be represented by $E(q)$, which is the electromagnetic wave on the arbitrarily closed surface S surrounding p, which is shown in Fig. 1. Boundary integral equation can be written as:

$$\alpha E(p) = \frac{1}{4\pi} \iint\limits_S \left[G(p,q) \frac{\partial E(q)}{\partial \mathbf{n}} - E(q) \frac{\partial G(p,q)}{\partial \mathbf{n}} \right] dS \tag{2}$$

where G is Green function, $\mathbf{n}$ the outward normal vector on S, α the coefficient of position, when the measuring surface is located outside the source, and $\alpha = 1$.

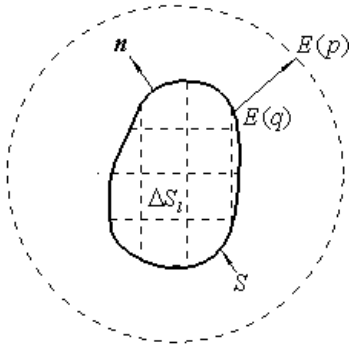

Figure 1. Active radiation boundary integral.

Now S is divided into L subunits. Each unit is ΔS_l, and the number of nodes is K (K is 6 or 8). Discreting Equation (2), the following equation can be obtained:

$$E(p)=\sum_{l=1}^{L}\frac{1}{4\pi}\iint_{\Delta S_l}\left[G(p,q_\xi)\frac{\partial E(q_\xi)}{\partial \mathbf{n}}-E(q_\xi)\frac{\partial G(p,q_\xi)}{\partial \mathbf{n}}\right]dS \quad q_\xi\in\Delta S_l \quad (3)$$

where q_ξ is the local coordinate on the sub-unit. By introducing the interpolation function $X_m(q_\xi)$, the boundary value $E(q_\xi)$ at any position of the sub-unit can be expressed by the boundary value $E_{l,m}$ on the k node. That is:

$$\begin{aligned}E(p)&=\sum_{l=1}^{L}\frac{1}{4\pi}\iint_{\Delta S_l}\left[G(p,q_\xi)\sum_{k=1}^{K}\frac{\partial E_{l,k}}{\partial \mathbf{n}}X_k(q_\xi)-\sum_{k=1}^{K}E_{l,k}X_k(q_\xi)\frac{\partial G(p,q_\xi)}{\partial \mathbf{n}}\right]dS\\&=\sum_{l=1}^{L}\sum_{k=1}^{K}\frac{\partial E_{l,k}}{\partial \mathbf{n}}\frac{1}{4\pi}\iint_{\Delta S_l}G(p,q_\xi)X_k(q_\xi)dS\\&\quad-\sum_{l=1}^{L}\sum_{k=1}^{K}E_{l,k}\frac{1}{4\pi}\iint_{\Delta S_l}X_k(q_\xi)\frac{\partial G(p,q_\xi)}{\partial \mathbf{n}}dS \quad (4)\end{aligned}$$

It is supposed that there are N nodes on S. To simplify the expression, the boundary values of each node are re-composed of $N\times 1$ column vector $\mathbf{e}_q$. Its normal partial derivative is column vector $\mathbf{e}_q^{\mathbf{n}}$. N measuring points on the holographic surface are composed of $N\times 1$ column vector $\mathbf{e}_p$. Then Equation (4) is discrete and expressed as:

$$\mathbf{e}_p=\mathbf{A}\mathbf{e}_q^{\mathbf{n}}-\mathbf{B}\mathbf{e}_q \quad (5)$$

where $\mathbf{A}$ and $\mathbf{B}$ are $N\times N$ matrices. There are two unknown quantities in Equation (5), and a constraint equation must to be added.

If the holographic surface is the source surface S, $\mathbf{e}_p = \mathbf{e}_q$ and $\alpha = 1$. That is:

$$\alpha \mathbf{e}_p = \mathbf{A}_s \mathbf{e}_q^{\mathbf{n}} - \mathbf{B}_s \mathbf{e}_q \tag{6}$$

Be simplified:

$$\mathbf{e}_q^n = \mathbf{A}_s^{-1}(\alpha \mathbf{I} + \mathbf{B}_s)\mathbf{e}_q \tag{7}$$

where $\mathbf{I}$ is the unit matrix. According to Equations (5) and (7), we obtain the following equation:

$$\mathbf{e}_p = [\mathbf{A}\mathbf{A}_s^{-1}(\alpha \mathbf{I} + \mathbf{B}_s) - \mathbf{B}]\mathbf{e}_q = \mathbf{G}\mathbf{e}_q \tag{8}$$

where $\mathbf{G}$ is defined as the transfer matrix, which is the key of imaging. The imaging formula is:

$$\mathbf{e}_q = \mathbf{G}^{-1}\mathbf{e}_p \tag{9}$$

There is space shift invariance and linear characters about transfer matrix $\mathbf{G}$, but they do not guarantee its full rank. Its inverse matrix cannot be obtained directly. In order to ensure the stability of imaging, the singular value decomposition is often used. That is:

$$\mathbf{G} = \mathbf{U}\mathbf{\Sigma}\mathbf{V}^H \tag{10}$$

where $\mathbf{U}$ and $\mathbf{V}$ are unitary matrices, and $\mathbf{\Sigma}$ is a diagonal matrix.

$$\mathbf{\Sigma} = \mathrm{diag}(\sigma_1, \sigma_2, \sigma_3, \ldots, \sigma_N) \quad \sigma_1 \geq \sigma_2 \geq \sigma_3 \ldots \geq \sigma_N \tag{11}$$

where σ_n is the singular value of the matrix. So the imaging formula is:

$$\mathbf{e}_q = \mathbf{V}\mathbf{\Sigma}\mathbf{U}^H\mathbf{e}_p \tag{12}$$

3. DSBPM IMAGING ALGORITHM

In this paper, DSBPM is used to calculate the transfer matrix. Through default particular solution source, the particular solution matrix is obtained, and the transfer matrix can be calculated indirectly. These problems about variable interpolation, singular integral treatment, non-unique solution and large calculation can be avoided effectively in DSBPM [7].

The specific method is that the particular solution source is set in the departure from the boundary nodes' normal direction d. For each particular solution source, a particular solution to meet the Helmholtz boundary integral equation can be obtained in the source surface and the holographic measurement surface nodes. Vectors $\mathbf{e}_q^*$ and $\mathbf{e}_p^*$ are formed, and the following equation can be obtained:

$$\mathbf{e}_p^* = \mathbf{G}\mathbf{e}_q^* \tag{13}$$

The $N \times N$ particular solution matrices $\mathbf{E}_q^*$ and $\mathbf{E}_p^*$ are composed of the particular solution vector, produced by all particular solution sources. Each column in the particular solution matrix is a particular solution, i.e.,

$$\mathbf{E}_p^* = \mathbf{G}\mathbf{E}_q^* \tag{14}$$

Further transfer function $\mathbf{G}$ can be obtained as follows:

$$\mathbf{G} = \mathbf{E}_p^* \left(\mathbf{E}_q^*\right)^{-1} \tag{15}$$

If the test data $\mathbf{e}_p$ is known in the holographic surface, the imaging formula is:

$$\mathbf{e}_q = \mathbf{E}_q^* \left(\mathbf{E}_p^*\right)^{-1} \mathbf{e}_p \tag{16}$$

There are two key points in DSBPM. One is the choice of the particular solution source and the other the choice of d. Generally, there are three types of particular solution sources: point source; plane source (such as metal circular plate); body source (such as spheres, triangular body). The particular solution sources are located in a certain distance away from the target surface boundary nodes' normal direction. The particular solution of transfer matrix on the boundary nodes can form a particular solution matrix to meet the system equations. The choice of d should be considered generally. If d is too small and near the nodes, it will increase the singularity interference and reduce the accuracy. If d is too big, it will bring instability in the particular solution matrix calculation. The experience formula is as follows [8]:

$$d = \frac{2lr}{\sqrt{l^2 + \beta r^2 \pm l}} \tag{17}$$

where l is the distance between nodes, r the radius of curvature of the boundary, β the experience coefficient, and $\beta = 0.002 \sim 0.02$. If the boundary is plane, $r \to \infty$, $d = 2l/\sqrt{\beta}$.

In the process of the target imaging, due to the interference of the surrounding environment and the inherent defects of the transceiver system, there are errors about the amplitude and phase of the holographic surface measurement. If these data are directly used to the target image reconstruction, there is a large deviation to the inversion results. Further analysis of factors affecting the inversion image is necessary. According to [9], the key parameter on the inversion results is the condition number $\text{cond}(G) = \sigma_1/\sigma_N$, in which σ_N is matrix minimum singular value. If σ_N is small, the condition number is very large. The measurement error of the holographic surface will be increased in multiples of the condition number, and the final inversion of the image loses authenticity. The analysis results are shown in Fig. 2, which analyzes the impact of system parameter settings on the condition number and chooses three groups of system parameters:

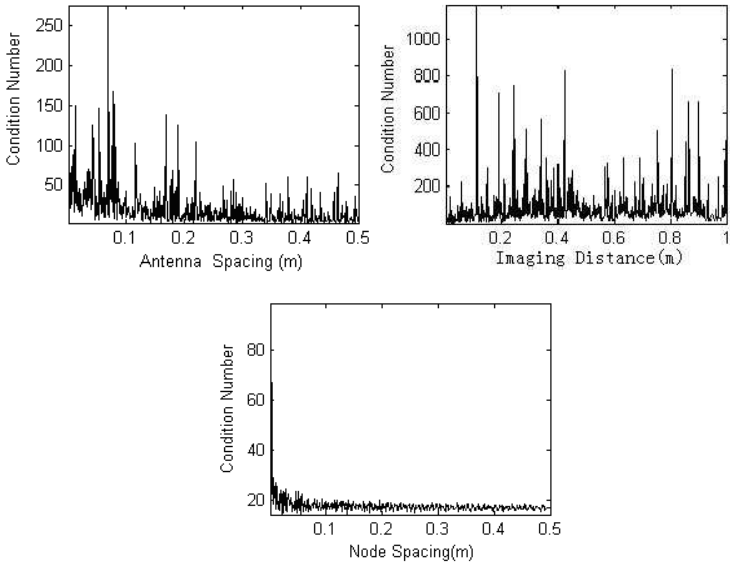

Figure 2. Effect of various parameters on the transfer matrix condition number.

the detection antenna array element spacing, target imaging distance, and target boundary node distance.

It can be obtained from Fig. 2 that the impact of antenna spacing and imaging distance is like random noise to condition number. Imaging distance can make inversion errors increase 1,000 times, and the inversion result has no value. If the detection target is going to be imaged accurately, the inversion error must be suppressed. Suppression methods will be discussed in the next section. Node spacing has almost no effect on the condition number, which can guarantee the robustness of the imaging when the target size is larger than the receiving antenna array and reflects the superiority of the BEM for large target imaging.

4. SIMULATION AND EXPERIMENT

Next, the imaging simulation experiment is carried out. The simulation conditions are: wavelength $\lambda = 8\,\text{mm}$; narrow-band two-dimensional plane imaging; the receiving antenna is a 50×50 plane array; the minimum distance between array elements is 5 mm; the distance to the target plane is 1 m. The target is a stereo hemisphere whose radius is 0.2 m. The division of the stereo hemispherical surface is shown in Fig. 3. Azimuth and elevation angles are divided into same

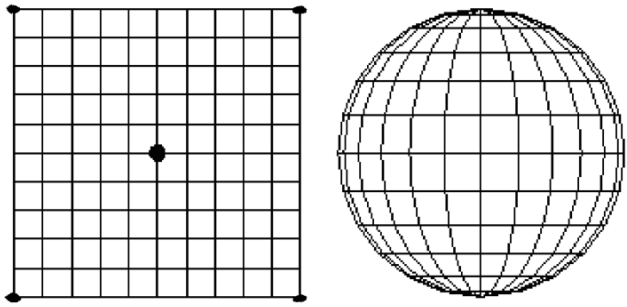

Figure 3. Schematic diagram of BEM grid division about the target. (a) Showed in plane. (b) Stereo hemispherical surface.

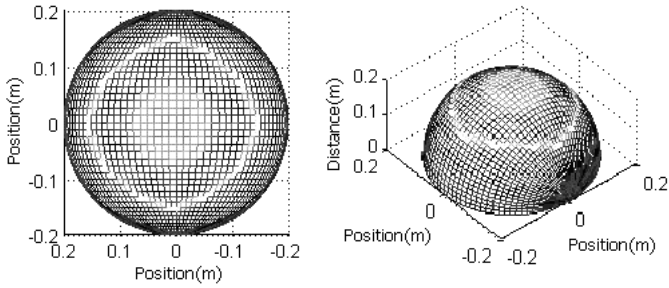

Figure 4. Short-range millimeter-wave holographic image of the stereo hemispherical surface. (a) The target inversion image. (b) Simulated three-dimensional image.

interval within π radian, and the total is 2402 nodes. In order to match the antenna array, the two nodes in north and south poles of the hemisphere are viewed as a collection of 50 nodes.

According to the echo signal amplitude and phase receiving, the transfer matrix is determined by the DSBPM, and the stereo hemispherical target is imaged. The imaging results are shown in Fig. 4.

In order to observe the details of the imaging clearly, the radius 100 mm ring and radius 50 mm circle were added to the surface of the hemisphere. Fig. 3 shows that DSBPM algorithm is effective to short-range hemisphere surface target imaging. The inversion image accurately restores the stereo hemispherical shape and surface detail.

The following will focus on analyzing the impact of measurement error. To any point P in the target scattered field, the electromagnetic

field inversion error is defined as follows:

$$\varepsilon = \frac{\left\| E(p) - \hat{E}(p) \right\|}{\left\| \hat{E}(p) \right\|} \times 100\% \tag{18}$$

where $E(p)$ is the true value of the inversion signal and $\hat{E}(p)$ the theory value [10, 11]. Error analysis in the third section shows that measurement error will increase in multiples of the condition number. Fig. 2 shows the relationship between array element spacing and target distance, and the condition number is random. The choice of the parameters cannot avoid the impact of the condition number. A regularization method is introduced to reduce the error. Some white noise was added to the holographic measurement surface. It is observed that the sensitivity of the inversion results in the measurement noise and the treatment effect of the regularization method.

It is supposed that the holographic surface measurement data SNR is 20 dB and that the simulation conditions remain unchanged. The stereo hemispherical target is imaged. Fig. 5 shows the inversion image without regularization.

Figure 5 shows that the inversion image is different from the theoretical value. Hemisphere surface details diffuse seriously, and the ring and circular plane are blurred. Singular value truncation filtering method is proposed and used to deal with the inversion image. Through the above analysis, the increase of condition number is due to small singular value. Some of the smaller singular values assigned to zero directly eliminate their influence on the inversion error. Assumed that the filter model is:

$$f_i = \begin{cases} 1 & \sigma_i \geq \alpha\sigma_1 \\ 0 & \sigma_i \leq \alpha\sigma_1 \end{cases} \tag{19}$$

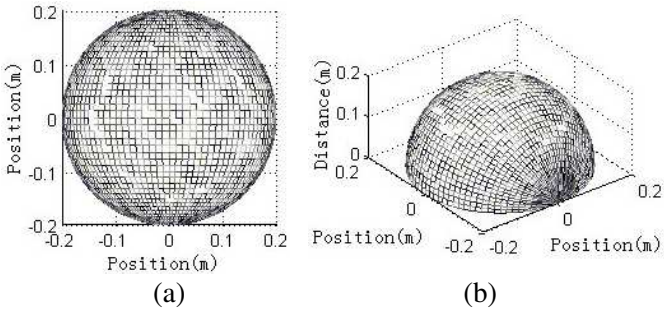

Figure 5. Short-range millimeter-wave holographic image affected by noise. (a) The target inversion image. (b) Simulated three-dimensional image.

where α is truncated coefficient ratio. The choice of α is very critical. If α is too small, it will reduce the imaging resolution, and if α is too large, it will not filter out the noise. Generally, it is determined by the actual measurement SNR. It is known that SNR of holographic surface measurement data are 20 dB, and all singular values below this range are filtered out. Assume that the singular value σ_{k+1} to meet:

$$20\log\left(\sigma_{K+1}/\sigma_1\right) < -20 \tag{20}$$

The truncated coefficient ratio can be calculated, that is $\alpha = 0.1$. Fig. 6. shows the inversion image after filtering.

Figures 5 and 6 are compared: after regularization, the measurement error has been suppressed effectively, and the image effect has been improved significantly. The ring and the circular plane of the hemisphere surface are also consistent with the theoretical values. The results show that the singular value truncation filtering method is simple and effective.

The BEM for short-range millimeter-wave holographic imaging is verified by the imaging system experiment [8, 12]. The test system

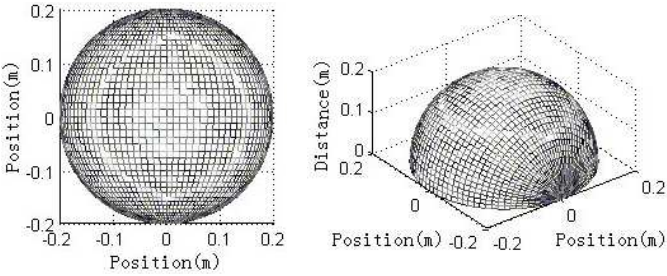

Figure 6. Short-range millimeter-wave holographic image after filtering. (a) The target inversion image. (b) Simulated three-dimensional image.

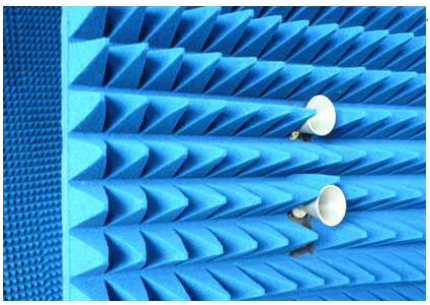

Figure 7. The picture of the test prototype working.

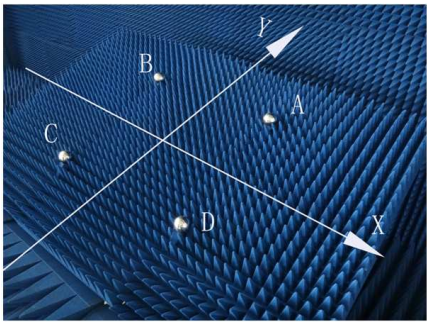

Figure 8. The picture of the actual target.

uses two close small horn antennas, as the transmitting and receiving antennas. The test prototype is fixed in the scanning frame and moving with the scanning frame. The target frame is composed of low reflectivity foam, and the height is 1.5 m. Fig. 7 is a picture of the test prototype.

The test parameters are as follows: the transmitting frequency is 35 GHz; the transmitting power is 10 dBm; the scanning plane is $0.5\,\text{m} \times 0.5\,\text{m}$ and samples 50 data points in the horizontal X-axis and vertical Y-axis; the sampling interval is 1 cm. The distance of the target and measuring surface is 1 m along the z-axis. The targets are 4 small metal balls whose radius is 5 cm. Fig. 8 is a picture of the actual target.

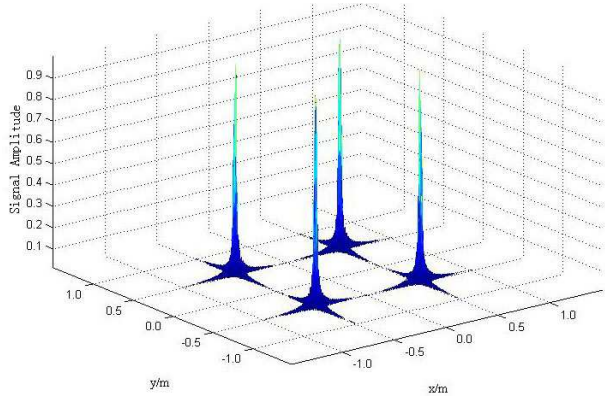

(a)

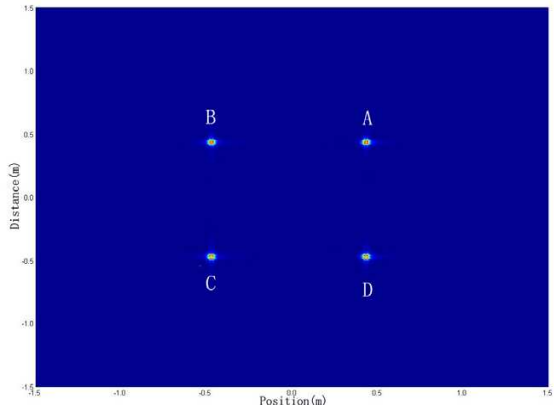

(b)

Figure 9. Inversion image of small metal balls. (a) Graphical representation of three-dimensional pulse. (b) Graphical representation of two-dimensional plane.

To simplify the algorithm, the target plane is divided into 49×49 square grids. The total is 50×50 nodes, which are consistent with the sampling points. The transfer matrix is established using DSBPM, and the target of the small balls is imaged. Regularization is used for the imaging results. The processed image is shown in Fig. 8, including three-dimensional pulse graphics and two-dimensional graphics.

It can be obtained from Fig. 9 that the side length of the target plane is 2 times of the scanning plane and that the short-range millimeter-wave holographic imaging using DSBPM obtains good results. As the target size is greater than the measuring surface, Gibbs effect and winding effect in Fourier transform algorithm have been very well controlled. The positional relationship of the ball target reflects the actual situation, and the intensity of the ball target image is the same basically. Imaging algorithm was proved to have good spatial resolution and high amplitude accuracy.

5. CONCLUSION

In this paper, BEM algorithm is presented firstly for short-range millimeter wave holographic imaging. DSBPM algorithm is introduced to calculate the transfer matrix and complete image inversion. This method can avoid variable interpolation, singular integral processing, non-uniqueness solution, etc., which greatly simplifies the computation process and promotes the practical process of BEM algorithm. The sensitivity of the measurement error to inversion image is analyzed. Singular value truncation filtering method is used to ensure the reality of the inversion image. Four small metal balls as the goal, the actual test was done. The result shows that DSBPM is effective for large target imaging and can obtain good spatial resolution and high amplitude accuracy.

ACKNOWLEDGMENT

This work was supported by the National Natural Science Foundation of China under Grant 61001010.

REFERENCES

1. McMakin, D. L., P. E. Keller, D. M. Sheen, et al., "Dual surface dielectric depth detector for holographic millimeter-wave security scanners," *SPIE Proceeding*, Vol. 7309, 73090G, 1–10, 2009.

2. Sheen, D. M., D. L. McMakin, W. M. Lechelt, et al., "Circularly polarized millimeter-wave imaging for personnel screening," *SPIE Proceeding*, Vol. 5789, 117–126, 2005.
3. Sheen, D. M., T. E. Hall, R. H. Severtsen, et al., "Active wideband 350 GHz imaging system for concealed-weapon detection," *SPIE Proceeding*, Vol. 7309, 73090I, 1–10, 2009.
4. McMakin, D. L., D. M. Sheen, and T. E. Hall, "Biometric identification using holographic radar imaging techniques," *SPIE Proceeding*, Vol. 6538, 65380C, 1–12, 2007.
5. Sheen, D. M., D. L. McMakin, and T. E. Hall, "Cylindrical millimeter wave imaging technique and applications," *SPIE Proceeding*, Vol. 6211, 62110A, 1–10, 2006.
6. Keller, P. E., D. L. McMakin, and D. M. Sheen, "Privacy algorithm for cylindrical holographic weapons surveillance system," *IEEE Aerospace and Electronic Systems Magazine*, Vol. 15, No. 2, 17–24, 2000.
7. Lettington, A. H., M. P. Rollason, and S. Tzimopoulou, "Image restoration using a two dimensional Lorentzian probability model," *Journal of Modern Optics*, Vol. 47, No. 5, 931–938, 2000.
8. Zhang, S. Y. and X. Z. Chen, "The boundary point method for the calculation of exterior acoustic radiation problem," *Journal of Sound and Vibration*, Vol. 228, No. 4, 761–772, 1999.
9. Bi, C. X., "Theoretical and experimental study on the distributed source boundary point method based nearfield acoustic holography," Hefei University of Technology Doctoral Thesis, 35–51, Hefei, 2004.
10. Xu, L., X.-Z. Chen, C.-X. Bi, et al., "Nearfield acoustic holography resolution enhancing method based on interpolation using orthogonal spherical wave source," *Journal of Zhejiang University (Engineering Science)*, Vol. 43, No. 10, 1808–1811, 2009.
11. Deng, J.-H., X.-D. Liu, and Y.-C. Shan, "Research on evanescent wave and propagation wave in sound field and the improved acoustic holography method," *Technical Acoustics*, Vol. 28, No. 5, 565–571, 2009.
12. Zhang, L. X., N. J. Li, S.-F. Hu, et al., *Radar Scattering and Imaging Diagnostic Testing*, 145–220, China Astronautics Press, Beijing, 2009.